Journal of Integrative Neuroscience

J. Integr. Neurosci. **2026**; 25(8): 52353
https://doi.org/10.31083/JIN52353

Original Research

High-Definition Transcranial Direct Current Stimulation (HD-tDCS) Enhances Cognitive Recovery After Traumatic Brain Injury Through Synaptic PlasticityRelated Changes

Zijia Guo[1,†], Nan Bai[2,†], Wenxuan Xin[1], Maosheng Xiang[2], Yuanming Geng[2], Weiyi Xie[1], Chiyuan Ma[1,2,*]

[1]Jinling Clinical Medical College, Nanjing University of Chinese Medicine, 210023 Nanjing, Jiangsu, China
[2]Department of Neurosurgery, Nanjing Jinling Hospital, Affiliated Hospital of Medical School, Nanjing University, 210093 Nanjing, Jiangsu, China
*Correspondence: machiyuan_nju@126.com (Chiyuan Ma)
[†]These authors contributed equally.
Academic Editor: Jessica A. Filosa
Submitted: 28 March 2026 Revised: 21 May 2026 Accepted: 25 May 2026 Published: 26 August 2026

Abstract

Background: Traumatic brain injury (TBI) often leads to long-term cognitive deficits. High-definition transcranial direct current stimulation (HD-tDCS) is a non-invasive neuromodulation approach with potential to enhance cognitive recovery. However, the underlying mechanisms by which tDCS influences neural synapses following mild TBI remain unclear. In this study, we aimed to identify the optimal HD-tDCS intervention cycle for improving cognition after repetitive mild TBI (rmTBI) in mice and to elucidate synaptic mechanisms. **Methods:** Male C57BL/6J mice underwent mild closed-head injury and received HD-tDCS (0.5 mA, 20 min/day) over the right parietal cortex. Cognitive performance was evaluated after 5, 10, and 15 days of stimulation using Y-maze and novel object recognition tests. Synaptic protein expression (PSD-95, SYN, NMDAR, GluA1) and BDNF/TrkB/CREB signaling pathway components were assessed via Western blot, while c-Fos expression was examined by immunofluorescence staining. Dendritic spine density was examined using Golgi staining. In addition, exploratory molecular modeling was performed to assess potential interactions between electric fields and the BDNF-TrkB complex. Separately, to contextualize our experimental findings, we also analyzed the public single-cell RNA-sequencing dataset GSE180862 as part of the study design. **Results:** HD-tDCS improved learning and memory performance, with the 15-day protocol showing the most robust effects among the tested schedules at the same post-injury endpoint. Behavioral improvements were accompanied by increased expression of BDNF-associated signaling proteins, elevated synaptic marker levels, and enhanced dendritic spine density in the hippocampus. In the 15-day stimulation group, a numerical trend toward sustained cognitive benefit was observed at 2 weeks after the end of stimulation, although the difference did not reach statistical significance. Molecular modeling suggested potential field-protein interactions but did not establish direct conformational modulation *in vivo*. **Conclusions:** Cognitive recovery improved following HD-tDCS intervention, accompanied by upregulation of BDNF/TrkB/CREB pathway-related proteins, synaptic markers, and dendritic spine density. These findings suggest a close association between repeated HD-tDCS and plasticity-related molecular changes after brain injury, although causal evidence for pathway activation requires further investigation.

Keywords: transcranial direct current stimulation; brain injuries, traumatic; cognition; neuronal plasticity

1. Introduction

Traumatic brain injury (TBI) is one of the main causes of death and long-term disability worldwide [1]. The pathological process is complex, encompassing primary mechanical injuries as well as secondary injuries induced by inflammatory responses, oxidative stress, metabolic disorders, neuronal apoptosis, axonal fractures, and additional factors [2]. These biological cascade reactions can persist for several days to several weeks, leading to significant neural network disruption and cognitive and motor dysfunction. While existing clinical treatment strategies can mitigate acute injuries to some degree, effective interventions for secondary injuries and the promotion of nerve repair remain inadequate. Consequently, there is an urgent necessity to investigate novel treatment approaches that focus on the regulation of neural plasticity.

Among the numerous molecules influencing the prognosis and neural recovery following TBI, brain-derived neurotrophic factor (BDNF) has garnered significant attention due to its essential role in neuronal survival, axon regeneration, and synaptic plasticity [3]. Brain-derived neurotrophic factor (BDNF) activates signaling pathways, including phosphatidylinositol 3-kinase/protein kinase B (PI3K/Akt), mitogen-activated protein kinase/extracellular signal-regulated kinase (MAPK/ERK), and phospholipase C-γ (PLC-γ), through its interaction with the high-affinity receptor tropomyosin receptor kinase B (TrkB). This activation promotes neuronal survival, synaptic formation, and network remodeling [4]. Numerous studies have demonstrated that BDNF expression exhibits distinct phase-dependent changes following TBI. In the acute phase, BDNF levels typically decrease, a phenomenon associ-

ated with an intensified inflammatory response and exacerbated neuronal damage. In contrast, during the subacute to chronic stages, compensatory upregulation of BDNF may occur in certain brain regions, contributing to the recovery of plasticity after injury [5]. However, the significant differences among different degrees of injury, different brain regions, and different models suggest that the changing pattern of BDNF after TBI is complex and time-dependent [6], and its precise function in the recovery process of TBI has not been fully elucidated.

In recent years, the advent of non-invasive brain stimulation techniques has opened new avenues for the regulation of neural plasticity. Notably, transcranial direct current stimulation (tDCS) has garnered significant attention within the field of neurorehabilitation, owing to its safety, ease of application, and high repeatability [7]. tDCS can modulate the membrane potential of cortical neurons, alter the excitability of both local and distal networks, and induce long-term potentiation (LTP)-like plasticity changes through the application of low-intensity direct current [8]. Moreover, high-definition transcranial direct current stimulation offers significant advantages in current focusing and target accuracy, thereby enhancing the potential for targeted modulation of specific brain regions [9]. To enhance spatial concentration in the stimulation area and mitigate the limitations of current dispersion in traditional dual-electrode tDCS, we adopted a smaller-diameter ring electrode design based on research by Jung et al. [10]. Previous studies indicate that reducing electrode area or employing multi-electrode configurations can improve spatial focusing of the electric field to some extent, thereby enhancing the localization characteristics of current distribution [11]. Additionally, concentric electrodes have been proposed as an alternative to multi-electrode high-difinition stimulation schemes for optimizing current pathways and enhancing spatial selectivity [12].

Increasing evidence indicates that BDNF serves as a crucial molecular basis for tDCS-induced neuroplasticity [13]. Animal and clinical studies have demonstrated that anodic tDCS can upregulate the expression of brain-derived neurotrophic factor (BDNF) in the cortex and hippocampus. This stimulation enhances TrkB-mediated signaling pathways associated with synaptic plasticity and promotes axon growth, dendritic spine formation, and synaptic remodeling in neurons [14]. Meanwhile, the therapeutic effect of tDCS depends to some extent on the individual differences in the expression level of BDNF. For example, the polymorphism of brain-derived neurotrophic factor Val66Met (BDNF Val66Met) has been proved to significantly affect the sensitivity of tDCS in cognitive improvement [15]. Moreover, in the TBI animal model, tDCS was shown to diminish inflammatory responses, enhance the microstructure of brain tissue, elevate synaptic protein expression, and increase BDNF levels in the injured brain region, thereby facilitating the recovery of behavioral function [16]. Nevertheless, systematic experimental evidence regarding the ability of high-definition transcranial direct current stimulation (HD-tDCS) to precisely regulate the BDNF signaling pathway and enhance the prognosis of TBI remains insufficient.

In conclusion, the dynamic alterations of BDNF following TBI and its impact on the reconstruction of neural plasticity hold considerable research significance. Furthermore, tDCS/HD-tDCS may facilitate the recovery of brain function by modulating the BDNF-TrkB signaling network [17]. However, at present, the temporal characteristics of tDCS regulating BDNF, cell type specificity, and its role at different stages after injury are still not fully clarified [18]. Systematic elucidation of the regulatory mechanisms by which HD-tDCS influences neural networks, molecules involved in synaptic plasticity (e.g., BDNF, TrkB, CREB), and behavioral recovery following TBI will facilitate the optimization of stimulation parameters, define the ideal intervention window, and furnish a theoretical foundation for the development of more targeted neuroregulatory treatment strategies. This study explores the effects of different intervention durations (5, 10, and 15 days) of HD-tDCS on cognitive dysfunction in mice following repetitive mild traumatic brain injury (rmTBI), using a fixed stimulation paradigm (0.5 mA, 20 min/day). These findings represent an initial step toward identifying optimal stimulation parameters. Additionally, it examines the potential mechanisms through which HD-tDCS influences synaptic function in mice with rmTBI to enhance cognitive performance.

2. Materials and Methods

2.1 Experimental Procedures

A total of 192 male C57BL/6J mice, aged 6 weeks, were included in the study and randomly assigned to various experimental groups. We employed G*Power 3.1 software (Heinrich-Heine-Universität, Düsseldorf, Germany, http://www.gpower.hhu.de/) to determine the minimum required sample size. The sample size for each group was calculated based on the pole test latency reported in previous studies (n = 6/group, effect size f = 0.8, $\alpha = 0.05$, and $\beta = 0.2$) [19]. One week post-injury, the mice were anesthetized for 20 minutes each day, during which HD-tDCS (0.5 mA, 20 minutes) was administered daily to the targeted area of the cerebral cortex [20].

Briefly, the study consisted of three experimental phases (Phase 1, Phase 2, and Phase 3). In Phase 1 (behavioral and histological assessment of HD-tDCS effects), mice were divided into four groups (CON, TBI, CON+HD-tDCS, TBI+HD-tDCS; n = 12 per group), with 6 mice per group tested at day 13 and the remaining 6 at day 20 post-modeling. In Phase 2 (optimization of stimulation duration), five groups were used (CON, TBI, TBI+5d, TBI+10d, TBI+15d; total n per group ranging from 12 to 24 as detailed in the **Supplementary Material**), and each endpoint (behavior, histology) was assessed 6 mice per condition. In

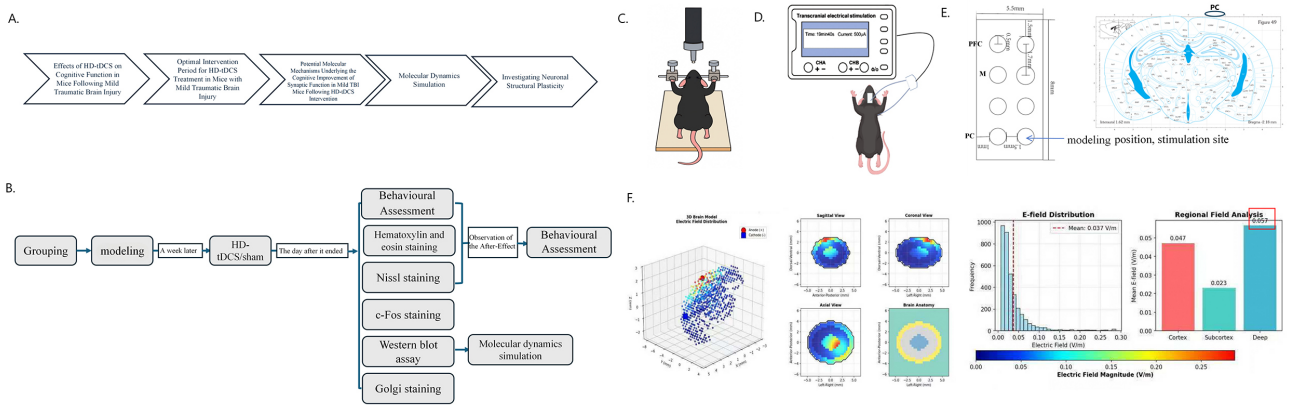

Fig. 1. Experimental design plan. (A) Experimental module diagram summarizing the study workflow. The relevance of each step (from rmTBI induction to behavioral testing) is to determine the optimal total stimulation duration (5, 10, or 15 days of daily HD-tDCS at 0.5 mA for 20 min/day) and to explore the associated synaptic signaling mechanisms (e.g., BDNF/TrkB/CREB pathway). Detailed experimental conditions, timing, and control groups are available in the **Supplementary Material**. (B) Experimental flowchart. (C) rmTBI modeling schematic diagram. (D) Schematic diagram of HD-tDCS intervention. (E) Electrode position. The stimulation electrode (anode) is located at the same coordinates as the mTBI impact site (right parietal cortex). Mouse brain section reproduced with permission from Franklin K.B.J. and Paxinos G., The Mouse Brain in Stereotaxic Coordinates, 3rd ed., Elsevier/Academic Press, 2008 [25]. (F) Simulation of HD-tDCS in mice. Electric field distribution was computed using a Python-based three-dimensional finite-voxel model with head geometry derived from the 15 μm average C57BL/6J mouse MRI model in Waxholm space. Schematic of the entire voxel; electric field distribution in the mouse brain under HD-tDCS stimulation (showing sagittal, coronal, and axial views, respectively, alongside anatomical brain diagrams); Average electric field strength (comparable to the deep electric field intensity observed in simulated human subjects undergoing HD-tDCS intervention at 2 mA stimulation parameters). HD-tDCS, high-definition transcranial direct current stimulation; PFC, prefrontal cortex; M, motor cortex; PC, parietal cortex; rmTBI, repetitive mild Traumatic brain injury; BDNF, brain-derived neurotrophic factor; TrkB, tropomyosin receptor kinase B; CREB, cAMP response element-binding protein.

Phase 3 (molecular mechanisms), four groups (CON, TBI, TBI+10d, TBI+15d; n = 12 per group) were used, with 6 mice per group allocated to Western blot and the other 6 to Golgi staining. For all comparisons, different mice were used at each time point (no repeated measurements on the same animal). Full group assignments, including exact numbers per experimental condition and per assay, are provided in the **Supplementary Material**.

First, we conducted an electric field simulation to predict the electric field strength reaching the deep brain regions of mice after applying HD-tDCS to the modeled location. The results showed that this field strength was comparable to that observed in humans when conventional 2 mA HD-tDCS stimulation was applied to the scalp and reached deep brain regions [21]. It is worth noting that Jackson et al. [20] had previously conducted relevant simulations and experimental verifications. Next, we conducted grouped experiments on mice. The specific experimental design and grouping are shown in Fig. 1A,B, and the **Supplementary Fig. 1**.

2.2 Animals

Six-week-old male C57BL/6J mice were obtained from the Laboratory Animal Center of Jinling Clinical Medical College, Nanjing University of Chinese Medicine (Nanjing, Jiangsu, China). All mice were housed under controlled temperature conditions with a 12-hour light/12-hour dark cycle and had free access to food and water.

2.3 Establishment of a Repetitive Mild TBI Mouse Model

Inducing mild closed-head injury in mice using the weight drop method (direct release of free weights onto the mouse scalp) [22]. After anesthesia induction with 1.25% tribromoethanol (2,2,2-tribromoethanol; catalog No. M2920, Nanjing Aibei Biotechnology Co., Ltd., Nanjing, Jiangsu, China), mice were secured in a stereotaxic apparatus (Jiangsu Sai'angsi Biotechnology Co., Ltd., Nanjing, Jiangsu, China). The right parietal lobe of mice was selected as the modeling site [23]. A 40 g weight was used for impact delivery from a height of 25 cm, repeated once daily for three consecutive days (Fig. 1C). Following modeling, the modified neurological severity score (mNSS) was employed to assess modeling success. All modeled mice scored within the mild injury range (1–6 points) [24]. Control group mice underwent anesthesia induction. Throughout the manuscript, the term "modeling" refers to the induction of repetitive mild TBI using the weight-drop method described above.

2.4 High-Definition Transcranial Direct Current Stimulation

The HD-tDCS device (Fig. 1D) is manufactured by Borui Kang Technology Co., Ltd (Beijing, China). Both the anode and cathode utilize custom Ag/AgCl electrodes with a radius of 0.5 mm. The effective contact area of each electrode was approximately 0.785 mm^2 (calculated as πr^2), yielding an electrode current density of approximately 637 A/m^2 (0.5 mA / 0.785 mm^2) and a charge density of approximately 764 kC/m^2 (current density × 1200 s) per session. These parameters are within the range commonly reported in rodent tDCS studies (Fig. 1E) (Ref. [25]). We placed the positive electrode at the modeling site, i.e., the parietal cortex (AP −2.18 mm, ML +1.25 mm from bregma), with the negative electrode positioned on the chest (**Supplementary Fig. 1**) [10]. To ensure precise and stable positioning, a custom acrylic plate serving as both a stereotaxic holder and an "electrode cap" was used. The plate had predrilled holes corresponding to the stimulation coordinates, through which the ring electrode was inserted to contact the scalp. A conductive paste was applied to both electrode sites to reduce skin–electrode impedance. Impedance was monitored in real time by the HD-tDCS device and maintained below 5 kΩ (indicated by a green light on the device screen) before each stimulation session. Current was ramped up linearly from 0 to 0.5 mA over 30 seconds, maintained at 0.5 mA for 20 minutes, and then ramped down from 0.5 mA to 0 over the final 30 seconds. After inducing anesthesia in mice with 1.25% tribromoethanol (In rodent tDCS studies, anesthesia was necessary to prevent stress-induced movement artifacts, ensure stable electrode contact, and avoid unnecessary suffering, in accordance with established animal welfare guidelines, e.g., IACUC and ARRIVE. Importantly, a comprehensive review by Jackson et al. [20] has demonstrated that anesthetics do not eliminate the neuromodulatory effects of tDCS, further supporting the validity of anesthetized protocols), HD-tDCS was applied continuously for 20 minutes at 0.5 mA. The non-HD-tDCS control group underwent the same anesthesia and electrode placement but received sham stimulation (current ramped up to 0.5 mA and immediately down to 0 within 1 minute, without sustained current delivery). One week after modeling, the 5-day group received HD-tDCS once daily for 5 consecutive days; the 10-day group received HD-tDCS daily for 5 consecutive days, followed by a 2-day stimulus-free interval, then HD-tDCS re-treatment for 5 days; the 15-day group followed the same protocol. To eliminate the influence of anesthesia as a confounding variable, all mice (including those in the 5-day and 10-day stimulation groups and all control groups) were anesthetized daily for a total of 15 days, matching the longest stimulation protocol. This ensured that all animals received identical anesthetic exposure, allowing any group differences to be attributed solely to the HD-tDCS intervention rather than to variations in anesthesia duration. All anesthetic injections used identical doses. The general health and well-being of the animals were monitored daily by measuring body weight throughout the stimulation period [26].

2.5 Mouse HD-tDCS Simulation

This simulation was performed as a methodological validation for Phases 1 and 2 to estimate the electric field distribution generated by our HD-tDCS protocol. The electric field induced by transcranial direct current stimulation (tDCS) was estimated using a Python-based three-dimensional voxel model (Python 3.x, Python Software Foundation, Wilmington, DE, USA) under the quasi-static approximation. A simplified mouse brain geometry was constructed based on MRI data (the 15 μm average wild-type C57BL/6J mouse MRI model in Waxholm space [27], which was generated from multiple C57BL/6J animals using 16.4T MRI and nonlinear averaging techniques, ensuring strain-appropriate anatomical geometry) and discretized into a 32^3–48^3 voxel grid (0.4 mm resolution), including cortical, subcortical, and deep brain regions.

Tissues were assumed to be homogeneous and isotropic, with conductivities of 0.33 S/m (cortex), 0.14 S/m (subcortex), and 0.33 S/m (deep regions). The electric potential φ was solved from: $\nabla\cdot(\sigma\nabla\phi) = 0$. The anode was placed over the right parietal cortex and the cathode at a thoracic reference site, corresponding to a total current of 0.5 mA. Dirichlet boundary conditions were applied at electrode sites, with zero-flux conditions elsewhere. The electric field was computed as $E = -\nabla\varphi$, and current density as $J = \sigma E$. A Gaussian filter was applied to reduce numerical noise. Peak and mean values of E and J within brain tissue were extracted for analysis.

To ensure plausibility, simulated electric field magnitudes were compared with previously reported ranges in rodent tDCS studies, showing consistent order of magnitude (Fig. 1F) [28].

2.6 Behavioral Tests

Behavioral tests were performed in Phase 1 and Phase 2 of the study. Behavioral testing (Fig. 2A) was conducted in a quiet room (light intensity <50 lx, temperature 22 ± 1 °C), with all animals acclimated in the test chamber for at least 30 minutes. All behavioral tests were performed by experimenters who were blind to the experimental groups/treatment conditions.

For the Y-maze novel arm test, the learning phase and exploration phase each lasted 5 minutes, with a 1-hour interval between them [29]. During the learning phase, one arm was randomly blocked with a baffle (designated as the novel arm), and each mouse was placed in one of the two accessible arms for 5 minutes of exploration. After a 1-hour delay, the baffle was removed, and the same mouse was placed at the distal end of the same starting arm for a 5-minute exploration phase. The ANY-maze video tracking system (version 7.0, Stoelting Co., Wood Dale, IL, USA)

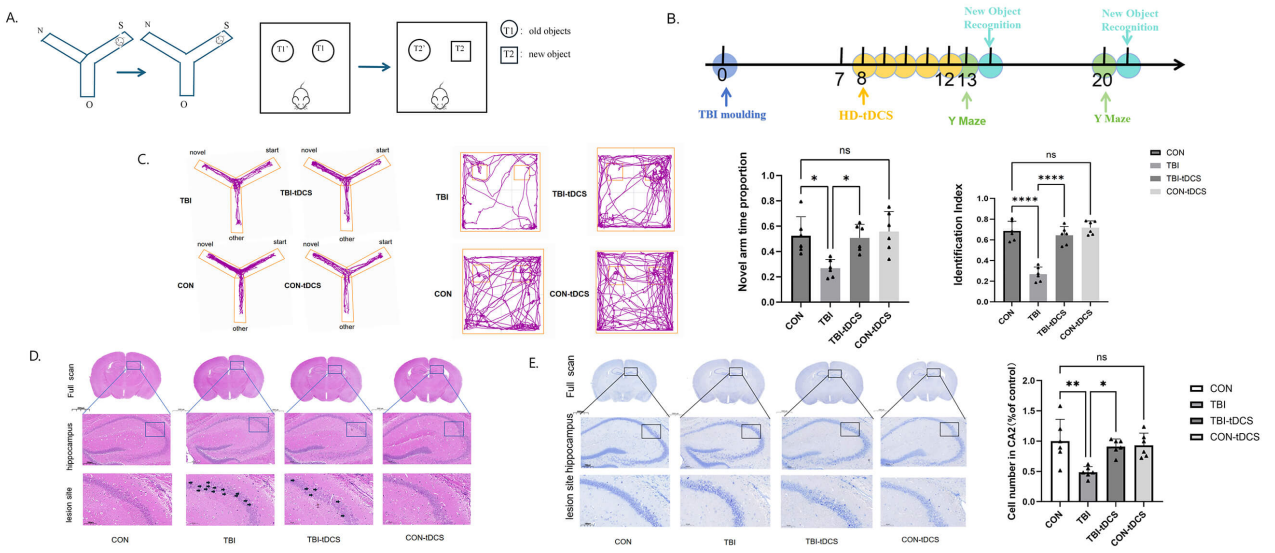

Fig. 2. Phase 1: Effects of HD-tDCS on cognitive function in mice following mild traumatic brain injury. (A) Schematic diagram of behavioral tests (the left side shows the Y-maze novel arm experiment, and the right side shows new object recognition) (B) Time axis of modeling, HD-tDCS application, and behavioral tests (C) Behavioral statistical analysis after 13 days. The proportion of novel arm time and recognition index in the TBI+HD-tDCS group were significantly increased, and they were higher than those in the TBI group. (D) After 13 days of H&E staining, HD-tDCS ameliorated neuronal damage and disorganization (black arrow). (E) Nissl staining at 13 days post-modeling showed that HD-tDCS increased the number of neurons in the injury area. All behavioral and cell number analyses (n = 6/group). Data are presented as means ± SEMs. *$p < 0.05$, **$p < 0.01$, and ****$p < 0.0001$ vs. each group using one-way analysis of variance with Tukey's test. ns, not significant. HD-tDCS, high-definition transcranial direct current stimulation; TBI, traumatic brain injury; SEM, standard error of the mean; Magnification: ×20, ×200, ×400; scale bar = 2000 μm, 200 μm, 100 μm.

was used to record the time spent in each arm during both phases. The proportion of time spent in the novel arm during the exploration phase relative to the total time spent in all three arms was calculated as the primary outcome measure (values range from 0 to 1) [29]. The protocol follows a standardized forced alternation Y-maze procedure with a novel arm retention interval, as detailed by Kraeuter et al. [30] and the International Mouse Phenotyping Resource of Standardised Screens (IMPC_YMZ_001) [31]. Briefly, the protocol includes the following features: (i) one arm was blocked during the learning phase (sampling trial), (ii) an inter-trial interval of 1 h was used, and (iii) the previously blocked arm was reopened during the exploration phase (choice trial) and designated as the novel arm.

For the novel object recognition (NOR) test, the learning phase and exploration phase each lasted 10 minutes, with a 1-hour interval between them. During the learning phase, each mouse was placed in an open field arena containing two identical cylindrical objects (placed 10 cm from the wall, designated T1 and T1′). The ANY-maze video tracking system recorded the total time the mouse spent exploring each object during the 10-minute learning phase. One hour later, one of the cylindrical objects was replaced with a novel cube-shaped object (the familiar cylindrical object was designated T2′, and the novel cube was designated T2), and the mouse was returned to the arena for a 10-minute exploration phase. The time spent exploring the novel object (T2) during the exploration phase was recorded. The recognition index was calculated as: Recognition index = T2 / (T2′ + T2). The index is expressed as a proportion (0–1 scale). Our protocol follows a widely used standardized NOR protocol (10 min sample phase, 1 h retention interval, 10 min test phase) as described by Maze Engineers [32]. The method is also consistent with general NOR applications reported in the literature [33]; however, key parameters are described explicitly in the main text to ensure reproducibility.

2.7 Histopathology and c-Fos Immunofluorescence Staining

Histological analyses (H&E, Nissl, and c-Fos immunofluorescence) were performed in Phase 1 and Phase 2 of the study, as detailed in the experimental design. Brain tissue was fixed in 4% paraformaldehyde (cat. no. G1101, Servicebio, Wuhan, Hubei, China) for 24 h and sectioned into 3-μm paraffin coronal slices. H&E staining used hematoxylin and eosin Y (cat. no. G1076, Servicebio) for 5 min and 20 s, respectively. Nissl staining used toluidine blue (cat. no. G1032, Servicebio) for 8 min. For immunofluorescence, sections were blocked with 3% BSA (cat. no. G5002-100G, Servicebio) /0.02% Triton-X100 (cat. no. G4004, Servicebio) and incubated with c-Fos antibody (Ta-

Table 1. Antibodies used for western blotting and immunofluorescence.

Protein	Primary Antibody	Catalog No.	Dilution	Manufacturer (Location)
NMDAR	Rabbit anti-NMDAR Monoclonal antibody	YM8881	1:5000	Immunoway (San Jose, CA, USA)
GluA1	Rabbit anti-GluA1 Monoclonal antibody	YM8615	1:3000	Immunoway (San Jose, CA, USA)
PSD-95	Rabbit anti-PSD-95 Monoclonal antibody	YM8292	1:5000	Immunoway (San Jose, CA, USA)
TrkB	Rabbit anti-TrkB Monoclonal antibody	ET7111-38	1:2000	Huabio (Hangzhou, Zhejiang, China)
CREB	Rabbit anti-CREB Monoclonal antibody	YM8342	1:5000	Immunoway (San Jose, CA, USA)
BDNF	Rabbit anti-BDNF Monoclonal antibody	YM8627	1:5000	Immunoway (San Jose, CA, USA)
GAPDH	Rabbit anti-GAPDH antibody	GB15004	1:4000	Servicebio (Wuhan, Hubei, China)
SYN	Rabbit anti-SYN Monoclonal antibody	YM8609	1:5000	Immunoway (San Jose, CA, USA)
β-actin	Rabbit anti-β-actin antibody	20536-1-AP	1:5000	Proteintech (Rosemont, IL, USA)
c-Fos	c-Fos Recombinant Rabbit Monoclonal Antibody	HA722666	1:1000	Huabio (Hangzhou, Zhejiang, China)

GAPDH, glyceraldehyde 3-phosphate dehydrogenase; β-actin, beta-actin; BDNF, brain-derived neurotrophic factor; CREB, cAMP response element-binding protein; SYN, synaptophysin; TrkB, tropomyosin receptor kinase B; PSD-95, postsynaptic density protein 95; NMDAR, N-Methyl-D-Aspartate receptor; GluA1, glutamate ionotropic receptor AMPA type subunit 1. Antibodies were purchased from Immunoway, Huabio, Servicebio, and ProteinTech, respectively, and all were diluted in 0.1% phosphate-buffered saline-Tween buffer.

ble 1) at 4 °C for 14 h, followed by Cy3 (cat. no. GB21303 for goat anti-rabbit IgG, Servicebio) or Alexa Fluor 488 secondary antibodies (cat. no. GB25301 for goat anti-mouse IgG, Servicebio). Dissection was performed according to the stereotaxic atlas of the standard mouse brain [25]. Following modeling, the primary cognitive-related lesion areas were analyzed, with damage predominantly concentrated in the hippocampal CA2 region. During this process, image processing software was employed to perform a simple and rapid semi-automated segmentation of mouse brain section images.

For quantitative analysis, brain sections were selected from bregma −1.5 mm to −3.0 mm covering the entire hippocampus. Every 5th section was sampled, yielding 5 coronal sections per animal. In each section, the hippocampal CA2 region was identified by overlaying the microscope image with a standard mouse brain atlas using Adobe Photoshop software (version CS6, Adobe Inc., San Jose, CA, USA). The region of interest (ROI) was manually delineated according to the atlas boundaries. Three non-overlapping fields of view were randomly selected within the ROI per section, giving 15 fields per animal. For Nissl-stained sections, healthy neurons (clear nucleolus, intact cell body) were manually counted by two blinded investigators. For c-Fos immunofluorescence, mean fluorescence intensity (integrated optical density/area) was measured using ImageJ (version 1.53, National Institutes of Health, Bethesda, MD, USA) after subtracting background from the corpus callosum. All image acquisitions and quantifications were performed by experimenters blinded to group allocation.

2.8 Golgi Stain

Brain samples were rinsed with ddH_2O and impregnated in a 1:1 mixture of Solution A and B for 6 hours at room temperature in the dark and refreshed for 14 days. Tissues were then transferred to Solution C for 24 hours and an additional 3 days in fresh Solution C. After embedding in OCT, 100 µm coronal sections were cut, mounted on slides, air-dried, and incubated in the working solution (Solution D:E:ddH_2O = 1:1:2) for 10 minutes. Sections were rinsed, dehydrated through graded ethanol, cleared in xylene (cat. no. 10023418, Sinopharm Chemical Reagent Co., Ltd., Shanghai, China), and cover-slipped with resin (cat. no. G1402, Servicebio, Wuhan, Hubei, China) for storage in the dark. Dendritic morphology was analyzed using Sholl analysis, and spine density was quantified using Neurolucida software (version 11.03, MBF Bioscience, Williston, VT, USA). For each animal, five neurons (one per selected section) were traced. Spine density was calculated as the number of spines per 10 µm dendrite length. All analyses were performed by investigators blinded to the experimental groups [34].

2.9 Bioinformatic Analysis of Public Datasets

To evaluate the transcriptional landscape of the BDNF signaling pathway following rmTBI and to provide a reference for the changes observed after HD-tDCS, we incorporated a public single-cell RNA-sequencing dataset into our study design. This dataset profiles the hippocampus and frontal cortex of mice at 24 h (acute) and 7 days (subacute) after mild TBI, which aligns with the injury model and the intervention window of our experiments. To independently assess transcriptomic changes in the BDNF signaling pathway after TBI, we analyzed a publicly available single-cell RNA sequencing dataset (GSE180862) from the Gene Expression Omnibus (GEO) database [35]. This dataset is derived from a separate cohort of mice that did not receive HD-tDCS intervention and serves as a complementary reference, not as part of the main experimental groups described above. This dataset comprises 44 samples, including traumatic brain injury (TBI) and sham surgery con-

trol groups, covering different time points (24 hours, 7 days) and brain regions (hippocampus, frontal cortex). Raw single-cell RNA sequencing data were processed using the Seurat software package (v4.3.0, Satija Lab, New York, NY, USA) [36]. Batch effects across samples were corrected using the Harmony algorithm [37]. Cells were clustered based on the Shared Nearest Neighbor (SNN) modular optimization algorithm. A BDNF signaling pathway gene set comprising 60 genes was defined using annotations from KEGG and GO databases. Differential expression analysis was performed using the FindMarkers function in Seurat, with the Wilcoxon rank sum test applied (default setting). The expression matrix of BDNF pathway genes was extracted from all cells, and the Pearson correlation coefficients among the genes were calculated. A gene co-expression network was then established using a correlation matrix with a threshold greater than 0.3. Additionally, Gene Ontology (GO) biological process enrichment analysis was performed for each community within the co-expression network. All statistical analyses were conducted in the R programming environment (v4.3.1). Data are presented as mean ± standard deviation. Suitable statistical tests were employed for group comparisons, with a p-value of less than 0.05 deemed statistically significant.

2.10 Western Blotting

The brains were carefully removed, and the right hippocampal region of each brain was rapidly dissected on ice. Total protein was extracted from brain tissue using RIPA buffer. Protein concentration was determined using the BCA Protein Assay Kit (Beyotime Biotechnology, Shanghai, China). The protein lysates were loaded onto a 10% sodium dodecyl sulfate-polyacrylamide gel electrophoresis (SDS-PAGE) gel and then transferred to polyvinylidene fluoride (PVDF) membranes (cat. no. G6015-0.45, Servicebio). The membranes were blocked with 5% skim milk buffer (cat. no. GC310001-500g, Servicebio) for 2 hours at room temperature, followed by overnight incubation at 4 °C with primary antibodies against GAPDH, β-actin, BDNF, CREB, SYN, TrkB, PSD-95, NMDAR, and GluA1 (Table 1). After washing three times for 5 minutes each in Tris-buffered saline (TBS) (cat. no. G0001-2L, Servicebio) containing 0.1% Tween 20 (TBST), the membrane was incubated with horseradish peroxidase (HRP)-conjugated secondary antibody (cat. no. GB23301, Servicebio) at room temperature for 2 hours. After three washes, the bands were detected using an enhanced chemiluminescence system, and relative gray values were analyzed using ImageJ software (version 1.53, National Institutes of Health) [38].

2.11 Molecular Dynamics Simulation

This molecular dynamics simulation was performed as an independent computational analysis, separate from the three experimental phases (Phases 1–3). To complement our *in vivo* findings with a possible molecular-level explanation, we performed molecular dynamics simulations to examine whether the applied electric field could influence the conformation of the BDNF-TrkB complex. Molecular dynamics simulations [39] were accomplished using GROMACS 2023.3 and CHARMM36 [40] force fields. The initial structure was solvated and ionized by CHARMM-GUI for energy minimization and then balanced for 100 ps at 300 K (NVT) and 1 bar (NPT), respectively. The production simulation runs for 100 ns with a time step of 2 fs. The control group was not subjected to an electric field, while the experimental group was subjected to a static electric field of 0.05 V/nm along the Z-axis. Electrostatic interactions are calculated through PME.

The trajectory was analyzed after the periodic boundary effect was removed. Structural stability was assessed by calculating the root mean square deviation (RMSD) of the protein backbone. Protein compactness was evaluated using the radius of gyration (Rg). Solvent accessibility was measured by the solvent-accessible surface area (SASA). The binding tightness between BDNF and TrkB was assessed by calculating the intermolecular distance between the two proteins. Solvation energy was also calculated to evaluate the interaction between the protein complex and the solvent. All analyses were performed using GROMACS built-in tools. The representative structure at the end of the 100 ns production run was used for superimposition and comparison. Visualization was accomplished using PyMOL 2.5.0 [41].

All simulations were conducted in triplicate, with statistical analysis performed using Student's t-test ($p < 0.05$). The system's temperature, pressure, and energy convergence were employed to validate the stability and reliability of the simulations.

2.12 Statistical Analysis

All data were obtained from independent groups of animals (i.e., different mice were used at each time point; no repeated measurements on the same animal; for detailed group assignment at each time point, see **Supplementary Material**). Normality was assessed using the Shapiro–Wilk test, and homogeneity of variances was examined using Levene's test. For data meeting both assumptions (normal distribution and equal variances), one-way analysis of variance (ANOVA) was performed followed by Tukey's post hoc test for multiple comparisons. When normality or homogeneity of variances was violated, the Kruskal–Wallis test with Dunn's post hoc correction was used. For comparisons involving only two groups, independent-samples t-test (parametric) or Mann–Whitney U test (non-parametric) was applied as appropriate. All statistical tests were two-tailed, and a significance level of $p < 0.05$ was considered statistically significant. Data are presented as mean ± standard error of the mean (SEM). Group allocation was blinded to the experimenters performing behavioral and histological quantifications, and the group codes were broken only after

the completion of all statistical analyses. Statistical analyses were performed using GraphPad Prism 10.0 software (GraphPad Software, Inc., San Diego, CA, USA).

3. Results

3.1 Effects of HD-tDCS on Cognitive Function in Mice Following Mild Traumatic Brain Injury

In Phase 1, following HD-tDCS treatment of the lesion site in the mouse model, behavioral testing was conducted as outlined in the experimental timeline (Fig. 2B). Test results from four groups of mice—CON, TBI, CON+HD-tDCS (5 days), and TBI+HD-tDCS (5 days)—demonstrated that TBI mice undergoing HD-tDCS intervention exhibited superior behavioral test performance compared to non-intervened TBI mice at day 13 post-modeling (i.e., 1 day after the last HD-tDCS session). Both the Y-maze novel arm time and the novel object recognition index were significantly higher in the TBI+HD-tDCS group than in the TBI group ($p < 0.05$; Fig. 2C). Although no significant statistical difference was observed between the TBI+HD-tDCS and TBI groups at day 20 post-modeling, the stimulated group consistently showed numerically higher performance in both behavioral tests (Fig. 2C and **Supplementary Fig. 2A**). Meanwhile, no significant statistical differences were observed between the stimulated and control groups in normal mice, although the stimulated group showed a numerically higher overall performance ($p > 0.05$). No obvious burns or irritation were observed on the scalp or subcutaneous tissue at the stimulation site based on daily visual inspections performed immediately after each stimulation session and at the endpoint. In addition, histological examination of brain sections (H&E staining) revealed no signs of thermal injury or tissue damage in the cortex or deep brain structures (Fig. 2D and Fig. 3C). These observations support the safety of HD-tDCS under the current stimulation parameters (0.5 mA, 20 min/day, up to 15 days) (**Supplementary Fig. 2**).

Representative images of H&E and Nissl staining indicate that HD-tDCS normalizes neuronal damage and disruption (black arrows) (Fig. 2D and **Supplementary Fig. 2C,D**). Following HD-tDCS intervention in mice with mild traumatic brain injury, neuronal counts in the lesion area increased at both 13 and 20 days post-modeling, with statistically significant differences observed in both cases (Fig. 2E and **Supplementary Fig. 2C,D**). Furthermore, c-Fos staining demonstrated that electrical stimulation induced neuronal activation (**Supplementary Fig. 2B**). These findings indicate that HD-tDCS exerts a cognitive-enhancing effect in mice following mild traumatic brain injury.

3.2 Identifying the Optimal Total Stimulation Duration of HD-tDCS in Mild TBI Mice

In Phase 2, to investigate the effects of different total stimulation durations, we performed behavioral tests on TBI mice that received HD-tDCS for 5, 10, or 15 total days (with daily sessions of 0.5 mA for 20 min) at the same post-modeling time point, as illustrated in the experimental timeline (Fig. 3A). Comparative analysis revealed that the behavioral performance of mice in the TBI+HD-tDCS (15 days) group surpassed that of the TBI group, with a statistically significant difference observed ($p < 0.05$, Fig. 3B). Behavioral testing revealed that the TBI-tDCS (15d) group significantly outperformed the TBI group in both Y-maze and novel object recognition tests ($p < 0.05$), and also outperformed the TBI-tDCS (5d) group in the novel object recognition test ($p < 0.05$). No significant differences were observed for the 5-day or 10-day groups compared to TBI (Fig. 3B). Thus, the 15-day protocol produced the best outcomes.

From the perspective of the post-stimulation effect, it was observed that two weeks after the stimulation ended, the test levels between the TBI+HD-tDCS (5 days) group and the TBI group were similar. At the two-week follow-up, no statistically significant differences were detected between any of the stimulated groups and the TBI group, although the 15-day group showed a numerically higher performance level (**Supplementary Fig. 3A–C**).

Pathological examination revealed that the arrangement of neurons in the hippocampal region of the brain tissue from the TBI group was loose and disordered, accompanied by observable neuronal degeneration and an increase in pericellular space. In the injured area, there was an increase in neuronal shrinkage and nuclear condensation, along with morphological features indicative of neurodegeneration. Following HD-tDCS treatment, tissue damage showed improvement, and cell death was notably reduced. The proportion of neuronal apoptosis decreased, and the morphology of neurons progressively approached normalcy (Fig. 3C,D). Additionally, compared to the TBI and CON groups, the expression of c-Fos in mice increased following HD-tDCS intervention, with a statistically significant difference noted ($p < 0.001$, Fig. 3E), indicating that electrical stimulation resulted in neuronal activation.

3.3 Transcriptomic Baseline of the BDNF Pathway After TBI and Its Relevance to HD-tDCS Effects

This analysis is an independent bioinformatic reference, separate from the three experimental phases (Phases 1–3). As an independent reference for Phase 3, to establish a baseline for TBI-induced transcriptional changes in the BDNF pathway independent of any stimulation, we first analyzed a public single-cell RNA-sequencing dataset (GSE180862) from TBI mice that did not receive HD-tDCS intervention. This dataset does not include any HD-tDCS treatment; it serves solely to characterize the natural evolution of BDNF pathway expression after TBI. Analysis of differentially expressed genes between the sham and TBI groups at various time points revealed that the pathway core genes BDNF and CREB remained at reduced expression levels during the subacute phase following mouse TBI (Fig. 4A).

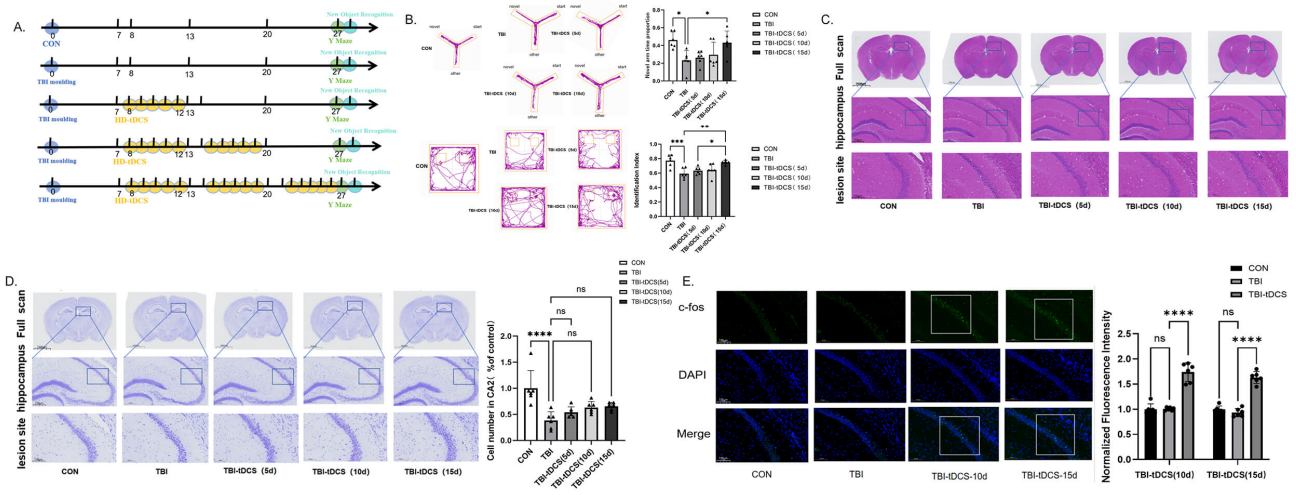

Fig. 3. Phase 2: Comparison of different stimulation durations (5, 10, or 15 days) of HD-tDCS in mice with mild TBI. (A) Timeline for exploring the optimal intervention cycle. (B) Statistical analysis of behavioral test results. Among the three stimulation schedules tested at the same post-injury endpoint, the 15-day group showed the best behavioral performance compared to the TBI group. However, because the interval from the last stimulation session to behavioral testing differed among the 5-, 10-, and 15-day groups, these findings should be interpreted with caution and do not establish a strict duration-dependent effect. (C) Hematoxylin and eosin (HE) staining. (D) Nissl staining and cell count bar graphs. (E) c-Fos staining and immunofluorescence intensity graphs. The significance brackets indicate the following pairwise comparisons: TBI+HD-tDCS vs. TBI ($p < 0.0001$) and TBI vs. CON (ns, not significant). Mice in the TBI+HD-tDCS group showed significantly increased c-Fos expression compared to the TBI group. All behavioral, cell count, and immunofluorescence intensity analyses (n = 6/group). Data are presented as means ± SEMs. *$p < 0.05$, **$p < 0.01$, ***$p < 0.001$, and ****$p < 0.0001$ vs. each group using one-way analysis of variance with Tukey's test. ns, not significant. HD-tDCS, high-definition transcranial direct current stimulation; TBI, traumatic brain injury; DAPI, 4',6-diamidino-2-phenylindole; Magnification: ×20, ×200, ×400; scale bar = 2000 μm, 200 μm, 100 μm.

GO enrichment analysis further highlighted that these genes predominantly associate with functions such as glutamatergic synaptic transmission, regulation of synaptic plasticity, and transsynaptic signal transduction. It is proposed that the disruption of the BDNF/TrkB pathway following TBI may directly influence the molecular underpinnings of learning and memory by modulating the function of glutamate receptors and the downstream CREB pathway (Fig. 4A). In comparison to the expression levels of altered genes in the control group, the TBI group exhibited overall inhibition, indicating that the injury significantly affected the molecular foundation of synaptic remodeling (Fig. 4A).

In Phase 3, current findings indicate that HD-tDCS was associated with increased expression of BDNF/TrkB/CREB pathway components and downstream synaptic proteins. This activation subsequently upregulates the expression of synaptic proteins (PSD-95, SYN) and associated receptors (NMDAR, GluA1) (Fig. 4B). Furthermore, this process exhibits a time-dependent nature, characterized as follows: After 10 days of electrical stimulation, BDNF levels and certain synaptic proteins initially increase, leading to a recovery of their functions. After 15 days of electrical stimulation, downstream proteins remain continuously activated, resulting in significant enhancements in synaptic structure and receptor function, as well as improvements in learning and memory capabilities (Fig. 4C).

3.4 Molecular Dynamics Simulation of the BDNF/TrkB Protein Complex

This simulation is an independent computational analysis, separate from the three experimental phases (Phases 1–3). To further investigate the effects of an applied electric field on the binding of essential proteins in the pathway, we selected the most classic and critical proteins. We systematically assessed the influence of the electric field on the conformational stability and energy state of the system. Additionally, we simulated the structural changes of the BDNF/TrkB protein complex before and after the application of the electric field.

The time series and distribution analyses of potential and kinetic energy indicate that the system attains thermodynamic equilibrium following initial fluctuations, regardless of the presence of an electric field. Both temperature and pressure exhibit fluctuations within a reasonable range, and the distributions of the two groups are comparable, suggesting that the system is stable and that the simulation settings are appropriate. The results of the RMSD analysis

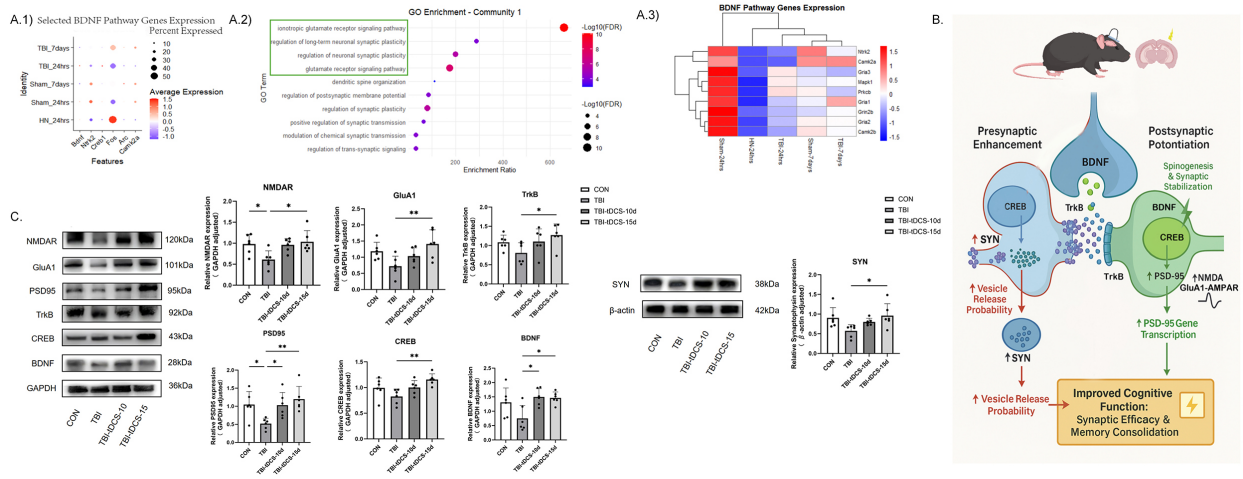

Fig. 4. Molecular correlates of HD-tDCS effects on synaptic proteins and cognitive function in mild TBI mice. (A) Bioinformatics analysis of GSE180862 data. (A.1) Differentially expressed genes between Sham and TBI groups at different time points. (A.2) Significantly enriched biological functions. (A.3) Heatmap comparing different groups, showing overall suppression in the TBI group. (A is based on the public dataset) (B) Hypothetical working model of HD-tDCS-mediated synaptic mechanisms in mild TBI mice, proposed based on our experimental data (Western blot, immunohistochemistry, and Golgi staining) and informed by the existing literature. The depicted cascades represent a conceptual framework requiring further functional validation. (C) Western blot analysis showing changes in the expression of BDNF/TrkB/CREB pathway-related proteins and downstream synaptic proteins following HD-tDCS (our experimental data). Abbreviations: TBI, traumatic brain injury; HD-tDCS, high-definition transcranial direct current stimulation; BDNF, brain-derived neurotrophic factor; TrkB, tropomyosin receptor kinase B; CREB, cAMP response element-binding protein; HN, hippocampus. Data were expressed as mean ± SEMs (n = 6/group). *$p < 0.05$, **$p < 0.01$.

demonstrate that the electric field increases the opening of molecular conformations, leading to a significant rise in the solvent-accessible surface area (SASA). This finding indicates that the electric field facilitates the exposure of molecules to the solvent environment. Additionally, under the influence of the electric field, the average distance between molecules decreases, signifying tighter binding. Further examination of solvation energy reveals that the solvation energy in the presence of an electric field is generally higher than that observed without it, implying that the electric field enhances the interaction between the solvent and the solute (Fig. 5A–C). Overall, the externally applied electric field under computer simulation did not alter the system's overall thermodynamic equilibrium but significantly influenced molecular stability and interactions. These results suggest that the electric field provides a potential explanation for the mechanism of tDCS action, namely by inducing molecular conformational rearrangements and enhancing molecular-solvent interactions to regulate the system's kinetic properties.

3.5 The Plasticity of Neuronal Structures

Data presented in this subsection are from Phase 3 of the study. The complexity of dendrites and the density of dendritic spines indicate the plasticity of neuronal structures. In Phase 3, using Golgi staining and Sholl analysis (see Methods; Fig. 6A), we examined neuronal morphology in the hippocampal CA2 region. As shown in Fig. 6B, region-specific alterations in dendritic complexity were observed. We examined the morphology of neurons in the hippocampus of mice, and the Sholl analysis demonstrated region-specific alterations in dendritic complexity. Compared with the CON group, the TBI group exhibited a significant reduction in the number of intersections within the 30–70 μm region ($p < 0.05$, Fig. 6B), while HD-tDCS treatment partially mitigated these deficits. Due to HD-tDCS intervention, the TBI-tDCS-10d and TBI-tDCS-15d groups exhibited significantly more dendritic intersections at 50 μm, 55 μm, and 60 μm from the cell body than the TBI group (50 μm, $p < 0.05$; 55 μm, $p < 0.05$; 60 μm, $p < 0.05$, Fig. 6B). Significant differences existed in the mean number of intersections across groups ($p < 0.01$, Fig. 6B), with the median in the TBI group being significantly lower than that in the CON group ($p < 0.01$, Fig. 6B). HD-tDCS treatment partially restored branching complexity, with the TBI-tDCS-15d and TBI-tDCS-10d groups showing significantly higher values than the TBI group ($p < 0.01$, Fig. 6B). Analysis of dendritic spine density revealed markedly increased hippocampal neuronal spine density in the TBI-tDCS-10d and TBI-tDCS-15d groups compared to the TBI group (10d group, $p < 0.05$; 15d group, $p < 0.01$), indicating that electrical stimulation enhances dendritic spine density in the hippocampal region of mice (Fig. 6C).

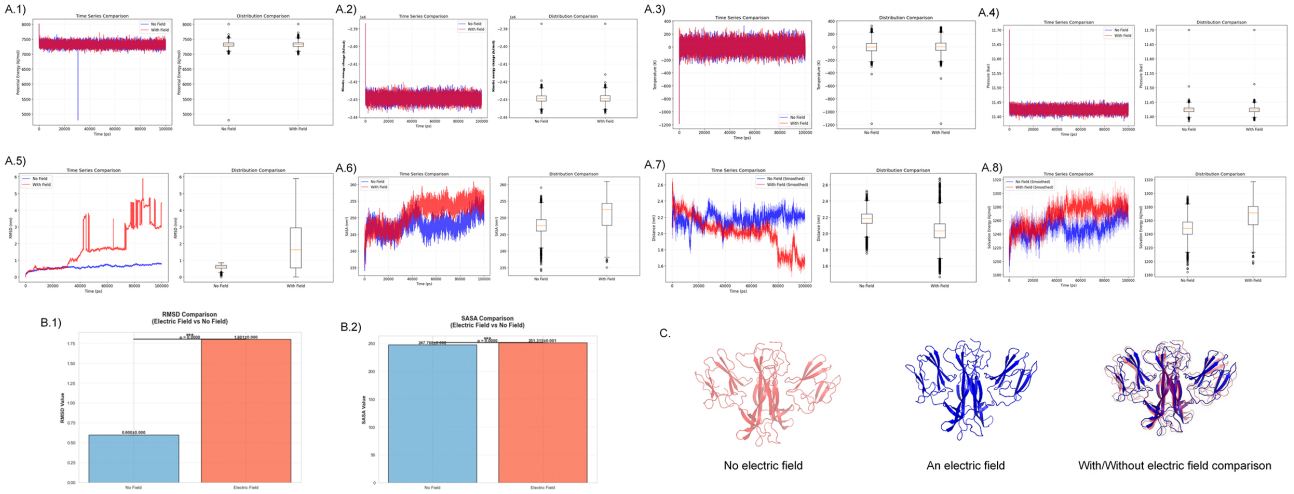

Fig. 5. Molecular dynamics simulation of the BDNF/TrkB protein complex. (A.1) Time series and distribution analysis of potential energy. (A.2) Time series and distribution analysis of kinetic energy changes relative to baseline. (A.3) Time series and distribution analysis of temperature. (A.4) Time series and distribution analysis of pressure. (A.5) Time series and distribution analysis of root mean square deviation (A.6) Time series and distribution analysis of solvent-accessible surface area. (A.7) Time series and distribution analysis of distance, i.e., binding compactness. (A.8) Time series and distribution analysis of solvation energy. (B.1) Statistical analysis of root mean square deviation (RMSD), a measure of structural stability. (B.2) Statistical analysis of solvent-accessible surface area. (C) Visualization of the BDNF/TrkB protein complex with and without an electric field. BDNF, brain-derived neurotrophic factor. TrkB, tropomyosin receptor kinase B. Data were expressed as mean ± SEMs. ***$p < 0.001$.

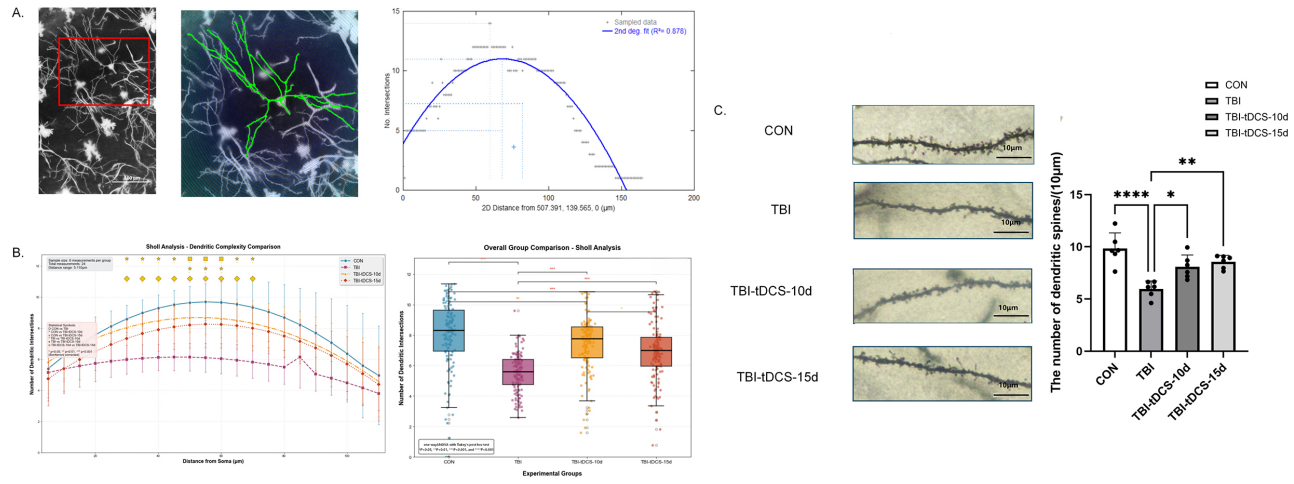

Fig. 6. Effects of HD-tDCS on neuronal structural plasticity in mild TBI mice. (A) Typical Golgi staining of hippocampal neurons. (B) Sholl analysis of dendritic branching complexity. For each animal, dendritic intersection counts were averaged across 5 randomly selected neurons per radius, and the resulting animal-level means were used for group comparisons (one-way ANOVA with Tukey's post hoc test, n = 6 animals/group). The TBI+HD-tDCS-10d and TBI+HD-tDCS-15d groups exhibited significantly more dendritic crossings at 50 μm, 55 μm, and 60 μm from the cell body compared to the TBI group. (C) Analysis of dendritic spine density in hippocampal neurons. Dendritic spine density in hippocampal neurons was significantly increased in the TBI+HD-tDCS-10d and TBI+HD-tDCS-15d groups compared to the TBI group. TBI, traumatic brain injury. HD-tDCS, high-definition transcranial direct current stimulation. Data were expressed as mean ± SEMs (n = 6/group). *$p < 0.05$, **$p < 0.01$, ***$p < 0.001$, ****$p < 0.0001$. The dashed curve in Fig. 6A represents a second-order polynomial fit ($R^2 = 0.878$) automatically generated by the ImageJ Sholl analysis plugin during data processing, included for visualization of the general dendritic branching trend.

4. Discussion

This study systematically assessed the impact of HD-tDCS on the cognitive function of mice with mild traumatic brain injury (TBI) and further investigated its potential mechanisms related to synaptic plasticity. Our primary findings are as follows: (1) HD-tDCS significantly enhances cognitive function in mice with mild TBI during the subacute stage; (2) Among the three stimulation schedules tested (5, 10, or 15 days of daily 0.5 mA for 20 min over the right parietal cortex), both the 5-day and 10-day protocols led to numerical improvements in cognitive performance that did not reach statistical significance compared to the TBI group. In contrast, the 15-day protocol produced significant cognitive improvement, and this effect persisted for about one to two weeks after the end of stimulation; (3) HD-tDCS may promote neuronal structural plasticity in conjunction with altered expression of BDNF/TrkB/CREB pathway components and synaptic proteins, although the causal direction remains to be determined; (4) Molecular dynamics simulations indicate that the applied electric field influences the stability of the protein complex by inducing conformational rearrangements and enhancing the solvent effect.

In behavioral testing, mice with traumatic brain injury (TBI) demonstrated marked cognitive improvement following high-definition transcranial direct current stimulation intervention, both in the Y-maze and novel object recognition tests. The 15-day HD-tDCS protocol produced the most pronounced effects after completing the full stimulation course (at day 27 post-modeling, since stimulation began 7 days after injury). In contrast, the Phase 1 study assessed a 5-day stimulation protocol at day 13 post-modeling. This aligns with prior research findings, which reported that HD-tDCS can enhance spatial learning and memory abilities following TBI through non-invasive electrical stimulation [42]. It is noteworthy that normal mice receiving HD-tDCS stimulation did not exhibit cognitive decline or behavioral abnormalities, further validating the safety and tolerability of HD-tDCS [43]. Nevertheless, ceiling effects in the Y-maze and NOR tasks (i.e., healthy mice may already perform near the maximum possible score) may have obscured any potential cognitive enhancement [44]. Studies using more challenging cognitive tasks have indeed observed enhanced performance in healthy mice after tDCS [45]. Comparative analysis of the three stimulation schedules revealed that the 15-day protocol produced the best performance at the tested endpoint among the schedules examined. In Phase 2 (all mice tested at day 27 post-TBI), the 15-day HD-tDCS protocol produced the best overall cognitive performance among the three stimulated groups. Specifically, it significantly outperformed the TBI group in both the Y-maze and novel object recognition tests, and also significantly outperformed the 5-day group in the novel object recognition test (Fig. 3B). This finding suggests that sustained electrical stimulation may facilitate its effects by cumulatively activating neural networks and promoting synaptic plasticity. Two weeks after stimulation, no statistically significant differences were detected between any of the stimulated groups and the TBI group. However, among the three stimulation schedules, the 15-day group consistently exhibited the highest numerical performance. This numerical trend suggests that a longer stimulation protocol may have the potential for sustained effects, although further investigation with larger sample sizes or more sensitive behavioral tasks would be needed to confirm this possibility.

By comparing various intervention cycles, we observed a clear time dependence in the cognitive improvement associated with HD-tDCS. The behavioral indicators of mice in the 15-day intervention group surpassed those in the 5-day and 10-day intervention groups, indicating that continuous electrical stimulation may enhance its effects by cumulatively activating neural networks and promoting synaptic plasticity. Furthermore, the aftereffects observed two weeks post-stimulation suggested that the advantages of a longer intervention period could be partially sustained, implying that HD-tDCS may facilitate long-term improvement through the persistent regulation of neural circuits [3,38]. Molecular dynamics simulations indicate that the applied electric field does not alter the overall thermodynamic equilibrium of the system. However, it increases the exposed surface area of BDNF/TrkB complexes, shortens intermolecular distances, and enhances solvent effects. This suggests that the electric field may enhance signaling pathway activity by inducing conformational rearrangements and modulating intermolecular interactions. While this provides a theoretical exploration of potential field-protein interactions, it does not imply direct conformational modulation *in vivo* and requires further *in vivo* validation.

Golgi staining and dendritic analysis revealed that HD-tDCS ameliorated deficits in hippocampal neuronal dendritic complexity and dendritic spine density in TBI mice. This indicates that HD-tDCS not only modulates molecular-level signalling but also promotes neuronal structural plasticity, thereby providing an anatomical basis for cognitive function recovery. An increase in dendritic spine density may enhance synaptic connectivity and information transmission efficiency, thereby improving learning and memory functions [46].

This study indicates that HD-tDCS, a non-invasive neuromodulation technique, can enhance cognitive function during the subacute phase of mild traumatic brain injury (TBI). By optimizing the intervention cycle and electrical field parameters and integrating these with behavioral rehabilitation training, the therapeutic effects are anticipated to improve further [47]. Furthermore, the combination of molecular dynamics simulations with behavioral and histological analyses provides integrated evidence for elu-

cidating the regulation of synaptic plasticity by HD-tDCS, thereby offering theoretical support for future clinical investigations.

Limitations

This study has several limitations. First, the efficacy of HD-tDCS was evaluated only in a mouse model of mild traumatic brain injury; it remains unclear whether similar effects occur in cases of moderate-to-severe TBI or during the chronic phase of injury. Second, although our data show a strong association between HD-tDCS and the upregulation of the BDNF/TrkB/CREB pathway, synaptic proteins, and dendritic spine density, these findings are correlational. There is a lack of causal evidence—such as pharmacological blockade of TrkB or genetic knockdown of BDNF—to determine whether this pathway is necessary or sufficient for the observed cognitive benefits. Third, our stimulation montage utilized a thoracic reference electrode. While this configuration follows established protocols, it may introduce current shunting through thoracic tissues and potentially modulate the peripheral autonomic nervous system. Although our sham-controlled group refutes the notion that nonspecific peripheral effects are the primary driver of recovery, future studies utilizing head-based reference electrodes (such as the contralateral cortex) will help distinguish between central and peripheral contributions. Fourth, our histological analysis focused primarily on the hippocampus; other cognition-related regions (such as the prefrontal cortex) were not systematically examined. Finally, further optimization of electric field parameters and intervention strategies is needed to enhance clinical translational value. Future studies combining multimodal neuroimaging, in vivo electrophysiology, and long-term follow-up will help address these gaps [48].

5. Conclusions

This study shows that HD-tDCS is associated with significant improvement in cognitive function during the subacute phase of rmTBI. This effect is correlated with increased expression of BDNF/TrkB/CREB pathway components, synaptic proteins, and enhanced dendritic spine density, suggesting that this signaling pathway may contribute to the observed cognitive improvement. Future studies using pharmacological or genetic manipulation of BDNF/TrkB signaling are warranted to establish causality. Furthermore, this effect is time-dependent. These findings provide both experimental and mechanistic support for the application of HD-tDCS in addressing cognitive impairment following TBI, thereby offering a theoretical foundation for future clinical translational research.

Availability of Data and Materials

The datasets used and analyzed during the current study are available from the corresponding author upon reasonable request.

Author Contributions

CM designed the research and edited the manuscript; ZG wrote the manuscript, performed research and analyzed the data; NB, WXin, MX, YG, WXie performed research, analyzed data, and contributed to drafting and revising the manuscript critically for important intellectual content. All authors contributed to editorial changes in the manuscript. All authors read and approved the final manuscript. All authors have participated sufficiently in the work and agreed to be accountable for all aspects of the work.

Ethics Approval and Consent to Participate

All experiments were approved by the Animal Ethics, Use, and Care Committee of Jinling Clinical Medical College, Nanjing University of Chinese Medicine (DZYJSKTW20251215001). All experiments were conducted in accordance with the guidelines described in the National Institutes of Health Guide for the Care and Use of Laboratory Animals and reported in accordance with the ARRIVE guidelines 2.0 (Animal Research: Reporting of In Vivo Experiments) (see **Supplementary Material**).

Acknowledgment

Not applicable.

Funding

This research was funded by the Jiangsu Provincial Department of Science and Technology (BE2022821).

Conflicts of Interest

The authors declare no conflicts of interest.

Supplementary Material

Supplementary material associated with this article can be found in the online version at https://doi.org/10.31083/JIN52353.

References

[1] Ziesel D, Nowakowska M, Scheruebel S, Kornmueller K, Schäfer U, Schindl R, et al. Electrical stimulation methods and protocols for the treatment of traumatic brain injury: a critical review of preclinical research. Journal of Neuroengineering and Rehabilitation. 2023; 20: 51. https://doi.org/10.1186/s12984-023-01159-y

[2] Jiang JY, Gao GY, Feng JF, Mao Q, Chen LG, Yang XF, et al. Traumatic brain injury in China. The Lancet. Neurology. 2019; 18: 286–295. https://doi.org/10.1016/S1474-4422(18)30469-1

[3] Hu E, Li T, Li Z, Su H, Yan Q, Wang L, et al. Metabolomics reveals the effects of hydroxysafflor yellow A on neurogenesis and axon regeneration after experimental traumatic brain injury. Pharmaceutical Biology. 2023; 61: 1054–1064. https://doi.org/10.1080/13880209.2023.2229379

[4] Murrough JW, Charney DS. Is there anything really novel on the antidepressant horizon? Current Psychiatry Reports. 2012; 14: 643–649. https://doi.org/10.1007/s11920-012-0321-8

[5] Rostami E, Krueger F, Plantman S, Davidsson J, Agoston D, Rising M. Alteration in BDNF and its receptors, full-length

and truncated TrkB and p75NTR following penetrating traumatic brain injury. Brain Research. 2014; 1542: 195–205. https://doi.org/10.1016/j.brainres.2013.10.047

[6] Han M, Zeng D, Tan W, Chen X, Bai S, Wu Q, et al. Brain region-specific roles of brain-derived neurotrophic factor in social stress-induced depressive-like behavior. Neural Regeneration Research. 2025; 20: 159–173. https://doi.org/10.4103/NRR.NRR-D-23-01419

[7] Ren B, Kang J, Wang Y, Meng X, Huang Y, Bai Y, et al. Transcranial direct current stimulation promotes angiogenesis and improves neurological function via the OXA-TF-AKT/ERK signaling pathway in traumatic brain injury. Aging. 2024; 16: 6566–6587. https://doi.org/10.18632/aging.205724

[8] Tien HH, Liu WY, Chen YL, Wu YC, Lien HY. Transcranial direct current stimulation for improving ambulation after stroke: a systematic review and meta-analysis. International Journal of Rehabilitation Research. Internationale Zeitschrift Fur Rehabilitationsforschung. Revue Internationale De Recherches De Readaptation. 2020; 43: 299–309. https://doi.org/10.1097/MRR.0000000000000427

[9] Chua EF, Ahmed R, Garcia SM. Effects of HD-tDCS on memory and metamemory for general knowledge questions that vary by difficulty. Brain Stimulation. 2017; 10: 231–241. https://doi.org/10.1016/j.brs.2016.10.013

[10] Jung DH, Lee JH, Lee HJ, Park JW, Jung YJ, Shin HK, et al. Therapeutic effects of a novel electrode for transcranial direct current stimulation in ischemic stroke mice. Theranostics. 2024; 14: 1325–1343. https://doi.org/10.7150/thno.90779

[11] Bikson M, Datta A, Rahman A, Scaturro J. Electrode montages for tDCS and weak transcranial electrical stimulation: role of "return" electrode's position and size. Clinical Neurophysiology : Official Journal of the International Federation of Clinical Neurophysiology. 2010; 121: 1976–1978. https://doi.org/10.1016/j.clinph.2010.05.020

[12] Bortoletto M, Rodella C, Salvador R, Miranda PC, Miniussi C. Reduced Current Spread by Concentric Electrodes in Transcranial Electrical Stimulation (tES). Brain Stimulation. 2016; 9: 525–528. https://doi.org/10.1016/j.brs.2016.03.001

[13] Reiss D, Nielsen L, Godfrey K, McEwen B, Power C, Seeman T, et al. Midlife reversibility of early-established biobehavioral risk factors: A research agenda. Developmental Psychology. 2019; 55: 2203–2218. https://doi.org/10.1037/dev0000780

[14] Boondam Y, Songvut P, Tantisira MH, Tapechum S, Tilokskulchai K, Pakaprot N. Inverted U-shaped response of a standardized extract of Centella asiatica (ECa 233) on memory enhancement. Scientific Reports. 2019; 9: 8404. https://doi.org/10.1038/s41598-019-44867-z

[15] Wiegand A, Nieratschker V, Plewnia C. Genetic modulation of transcranial direct current stimulation effects on cognition. Frontiers in Human Neuroscience. 2016; 10: 651. https://doi.org/10.3389/fnhum.2016.00651

[16] Yu W, Lin X, Gao S, Li C. Corrigendum to "Age-related changes of inactivating BK channels in rat dorsal root ganglion neurons" [J. Neurol. Sci 358 (1-2) (November 15 2015) 138-145]. Journal of the Neurological Sciences. 2016; 364: 200–201. https://doi.org/10.1016/j.jns.2016.02.001

[17] Jung DH, Ahn SM, Pak ME, Lee HJ, Jung YJ, Kim KB, et al. Therapeutic effects of anodal transcranial direct current stimulation in a rat model of ADHD. elife. 2020; 9: e56359. https://doi.org/10.7554/eLife.56359

[18] Li J, Zhai X, Yu C. Spatial distribution-based progression of spinal cord injury pathology: a key role for neuroimmune cells. Frontiers in Immunology. 2025; 15: 1505755. https://doi.org/10.3389/fimmu.2024.1505755

[19] Ahn SM, Jung DH, Lee HJ, Pak ME, Jung YJ, Shin YI, et al. Contralesional Application of Transcranial Direct Current Stimulation on Functional Improvement in Ischemic Stroke Mice. Stroke. 2020; 51: 2208–2218. https://doi.org/10.1161/STROKEAHA.120.029221

[20] Jackson MP, Rahman A, Lafon B, Kronberg G, Ling D, Parra LC, et al. Animal models of transcranial direct current stimulation: Methods and mechanisms. Clinical Neurophysiology : Official Journal of the International Federation of Clinical Neurophysiology. 2016; 127: 3425–3454. https://doi.org/10.1016/j.clinph.2016.08.016

[21] Alekseichuk I, Mantell K, Shirinpour S, Opitz A. Comparative modeling of transcranial magnetic and electric stimulation in mouse, monkey, and human. NeuroImage. 2019; 194: 136–148. https://doi.org/10.1016/j.neuroimage.2019.03.044

[22] Xiong Y, Mahmood A, Chopp M. Animal models of traumatic brain injury. Nature Reviews. Neuroscience. 2013; 14: 128–142. https://doi.org/10.1038/nrn3407

[23] Zhang LM, Zhang DX, Miao HT, Song RX, Shao JJ, Liu JZ, et al. Spautin-1 administration mitigates mild TBI-induced cognitive and memory dysfunction in mice via activation of caspase-3. International Immunopharmacology. 2023; 117: 109906. https://doi.org/10.1016/j.intimp.2023.109906

[24] Zhou M, Liu YW, He YH, Zhang JY, Guo H, Wang H, et al. FOXO1 reshapes neutrophils to aggravate acute brain damage and promote late depression after traumatic brain injury. Military Medical Research. 2024; 11: 20. https://doi.org/10.1186/s40779-024-00523-w

[25] Franklin KBJ, Paxinos G. The Mouse Brain in Stereotaxic Coordinates. 3rd ed. Elsevier/Academic Press: Amsterdam, Netherlands. 2008.

[26] Schwartz K, Pacharinsak C. Mouse Anesthesia and Analgesia. Current Protocols. 2024; 4: e1006. https://doi.org/10.1002/cpz1.1006

[27] Janke AL, Ullmann JFP. Robust methods to create ex vivo minimum deformation atlases for brain mapping. Methods (San Diego, Calif.). 2015; 73: 18–26. https://doi.org/10.1016/j.ymeth.2015.01.005

[28] Katoch N, Kim Y, Choi BK, Ha SW, Kim TH, Yoon EJ, et al. Estimation of brain tissue response by electrical stimulation in a subject-specific model implemented by conductivity tensor imaging. Frontiers in Neuroscience. 2023; 17: 1197452. https://doi.org/10.3389/fnins.2023.1197452

[29] Lou N, Zhu Y, Du X, Wang L, Tang H, Hu S, et al. Sex-specific behavioral changes in middle-aged mice. Scientific Reports. 2025; 15: 21992. https://doi.org/10.1038/s41598-025-05001-4

[30] Kraeuter AK, Guest PC, Sarnyai Z. The Y-Maze for Assessment of Spatial Working and Reference Memory in Mice. Methods in Molecular Biology (Clifton, N.J.). 2019; 1916: 105–111. https://doi.org/10.1007/978-1-4939-8994-2_10

[31] International Mouse Phenotyping Consortium. Y-maze protocol (IMPC_YMZ_001). IMPReSS: International Mouse Phenotyping Resource of Standardised Screens. Available at: https://www.mousephenotype.org/impress/ProcedureInfo?action=list&procID=955 (Accessed: 17 January 2026).

[32] Maze Engineers. Novel Object Recognition Test in Mice. ConductScience. Available at: https://maze.conductscience.com/novel-object-recognition-test-mice/ (Accessed: 17 January 2026).

[33] da Costa VF, Ramírez JCC, Ramírez SV, Avalo-Zuluaga JH, Baptista-de-Souza D, Canto-de-Souza L, et al. Emotional- and cognitive-like responses induced by social defeat stress in male mice are modulated by the BNST, amygdala, and hippocampus. Frontiers in Integrative Neuroscience. 2023; 17: 1168640. https://doi.org/10.3389/fnint.2023.1168640

[34] Barbati SA, Cocco S, Longo V, Spinelli M, Gironi K, Mattera A, et al. Enhancing Plasticity Mechanisms in the Mouse Motor Cortex by Anodal Transcranial Direct-Current Stimulation: The Contribution of Nitric Oxide Signaling. Cerebral Cortex (New

York, N.Y. : 1991). 2020; 30: 2972–2985. https://doi.org/10.1093/cercor/bhz288

[35] Arneson D, Zhang G, Ahn IS, Ying Z, Diamante G, Cely I, et al. Systems spatiotemporal dynamics of traumatic brain injury at single-cell resolution reveals humanin as a therapeutic target. Cellular and Molecular Life Sciences : CMLS. 2022; 79: 480. https://doi.org/10.1007/s00018-022-04495-9

[36] Hao Y, Hao S, Andersen-Nissen E, Mauck WM, 3rd, Zheng S, Butler A, et al. Integrated analysis of multimodal single-cell data. Cell. 2021; 184: 3573–3587.e29. https://doi.org/10.1016/j.cell.2021.04.048

[37] Korsunsky I, Millard N, Fan J, Slowikowski K, Zhang F, Wei K, et al. Fast, sensitive and accurate integration of single-cell data with Harmony. Nature Methods. 2019; 16: 1289–1296. https://doi.org/10.1038/s41592-019-0619-0

[38] Qi S, Liu X, Yu J, Liang Z, Liu Y, Wang X. Temporally interfering electric fields brain stimulation in primary motor cortex of mice promotes motor skill through enhancing neuroplasticity. Brain Stimulation. 2024; 17: 245–257. https://doi.org/10.1016/j.brs.2024.02.014

[39] Guan L, Qi B, Tan J, Chen Y, Sun Y, Zhang Q, et al. Structural Insight into the Inactive/Active States of 5-HT1AR and Molecular Mechanisms of Electric Fields in Modulating 5-HT1AR. Journal of Chemical Information and Modeling. 2025; 65: 2066–2079. https://doi.org/10.1021/acs.jcim.4c02278

[40] Huang J, Rauscher S, Nawrocki G, Ran T, Feig M, de Groot BL, et al. CHARMM36m: an improved force field for folded and intrinsically disordered proteins. Nature Methods. 2017; 14: 71–73. https://doi.org/10.1038/nmeth.4067

[41] Baugh EH, Lyskov S, Weitzner BD, Gray JJ. Real-time PyMOL visualization for Rosetta and PyRosetta. PloS One. 2011; 6: e21931. https://doi.org/10.1371/journal.pone.0021931

[42] Ahorsu DK, Adjaottor ES, Lam BYH. Intervention Effect of Non-Invasive Brain Stimulation on Cognitive Functions among People with Traumatic Brain Injury: A Systematic Review and Meta-Analysis. Brain Sciences. 2021; 11: 840. https://doi.org/10.3390/brainsci11070840

[43] Wong HL, Chan WC, Wong YL, Wong SN, Yung HY, Wong SMC, et al. High-definition transcranial direct current stimulation-An open-label pilot intervention in alleviating depressive symptoms and cognitive deficits in late-life depression. CNS Neuroscience & Therapeutics. 2019; 25: 1244–1253. https://doi.org/10.1111/cns.13253

[44] Schubiger MN, Fichtel C, Burkart JM. Validity of Cognitive Tests for Non-human Animals: Pitfalls and Prospects. Frontiers in Psychology. 2020; 11: 1835. https://doi.org/10.3389/fpsyg.2020.01835

[45] De Souza Nicolau E, Nogueira Souza AC, Freitas Rosa DV, Miranda DM, Romano-Silva MA. A rapid and efficient mouse model for transcranial direct current stimulation: enhanced cognitive performance and molecular alterations after anodal stimulation. Brain Stimulation. 2025; 18: 577–577. https://doi.org/10.1016/j.brs.2024.12.1052.

[46] Gipson CD, Olive MF. Structural and functional plasticity of dendritic spines – root or result of behavior? Genes, Brain, and Behavior. 2016; 16: 101–117. https://doi.org/10.1111/gbb.12324

[47] Alashram AR. Efficacy of combined transcranial direct current stimulation and computer-based cognitive rehabilitation on cognition in patients with traumatic brain injury: A systematic review. Applied neuropsychology. Adult. 2026. https://doi.org/10.1080/23279095.2026.2702490

[48] Radanovic A, Jamison KW, Kang Y, Tozlu C, Shah SA, Kuceyeski A. Longitudinal multimodal neuroimaging after traumatic brain injury. Human Brain Mapping. 2026; 47: e70534. https://doi.org/10.1002/hbm.70534